The EMBO Journal Vol.18 No.21 pp.5853–5862, 1999

Binding of the *Shigella* protein IpaA to vinculin induces F-actin depolymerization

Raphaëlle Bourdet-Sicard, Manfred Rüdiger[1,2], Brigitte M.Jockusch[1], Pierre Gounon[3], Philippe J.Sansonetti and Guy Tran Van Nhieu[4]

Unité de Pathogénie Microbienne Moléculaire and [3]Station Centrale de Microscopie Electronique, Institut Pasteur, 28 rue du Docteur Roux, 75724 Paris Cedex 15, France and [1]Cell Biology–Zoological Institute, Technical University of Braunschweig, Spielmannstrasse, D-38092 Braunschweig, Germany

[2]Present address: CARDIOGENE, Max-Planck-Strasse 15a, D-40699 Erkrath, Germany

[4]Corresponding author
e-mail: gtranvan@pasteur.fr

***Shigella flexneri*, the causative agent of bacillary dysentery, enters into epithelial cells by a macropinocytic process. IpaA, a *Shigella* protein secreted upon cell contact, binds to the focal adhesion protein vinculin and is required for efficient bacterial uptake. IpaA was shown here to bind with high affinity to the N-terminal residues 1–265 of vinculin. Using co-sedimentation and solid-phase assays, we demonstrated that binding of IpaA to vinculin strongly increases the association of vinculin with F-actin. We also characterized a depolymerizing activity on actin filaments associated with the vinculin–IpaA complex both *in vitro* and in microinjected cells. We propose that the conformational change of vinculin induced by IpaA binding allows interaction of the vinculin–IpaA complex with F-actin and subsequent depolymerization of actin filaments.**

Keywords: actin/bacterial invasion/IpaA/*Shigella flexneri*/vinculin

Introduction

Shigella flexneri, the causative agent of bacillary dysentery, is a Gram-negative bacterium that is able to enter into human epithelial cells. During the entry process, *Shigella* induces the formation of membrane extensions that result from polymerization of actin in the vicinity of the bacterium bound to the cell surface (Clerc and Sansonetti, 1987; Adam *et al*., 1995). These extensions rise around *Shigella* and fuse into membrane leaflets that engulf the bacterium in a large vacuole. A fine regulation of *Shigella*-induced cytoskeletal rearrangements allows the formation of a highly organized structure, called the entry focus, which is essential for efficient bacterial invasion. Several cytoskeletal proteins that are enriched specifically at the site of bacterial interaction with the cell participate in the organization of the entry focus. A vinculin-rich meshwork is observed at the level of the host membrane in intimate contact with the bacterium, forming a structure reminiscent of a focal adhesion (Tran Van Nhieu *et al*., 1997). Highly compacted actin filaments also associate with this structure. Membrane leaflets that surround the bacterium in the process of internalization are particularly enriched in actin-bundling proteins such as plastin and α-actinin (Adam *et al*., 1995; Tran Van Nhieu *et al*., 1997). At the peak of development of the entry focus, massive recruitment of ezrin, an actin-binding protein described as a cytoskeleton–membrane linker, is observed at the tip of *Shigella*-induced extensions (Skoudy *et al*., 1999), suggesting that ezrin may help to extend actin filaments during *Shigella* entry foci formation.

Shigella entry effectors are secreted upon cell contact by a type III secretion system encoded by the *mxi*/*spa* genes (Allaoui *et al*., 1992; Ménard *et al*., 1994). Type III secretion apparatus are found in numerous Gram-negative pathogenic bacteria and are thought to permit the translocation of bacterial effectors from extracellularly located bacteria into the cell cytosol (Hueck, 1998). In the case of *Shigella*, the Ipa proteins, which are secreted by the Mxi–Spa apparatus, are major determinants of the entry process. Actin polymerization at the site of bacterial interaction with the host cell is dependent on IpaB and IpaC, whereas IpaA allows the organization of actin polymerization into a structure that is productive for bacterial entry (Tran Van Nhieu *et al*., 1997). It was shown recently that a complex containing mostly IpaB and IpaC, and traces of IpaA and IpgD, has channeling activity across lipid bilayers *in vitro* (V.Cabiaux, personal communication). Also, IpaC was shown to induce actin polymerization and the formation of filopodia when introduced into the cell cytosol (Tran Van Nhieu *et al*., 1999). These data are consistent with the notion that IpaB and IpaC are directly responsible for actin polymerization at the site of *Shigella* entry, and may also allow translocation of other *Shigella* effectors involved in cytoskeletal reorganization, such as IpaA and IpgD. IpaA appears to modify the *Shigella*-induced entry foci; the disorganized filopodial protrusions that are observed in foci induced by an *ipaA* mutant organize into membrane leaflets in foci induced by wild-type *Shigella* (Tran Van Nhieu *et al*., 1997). The recruitment at the site of entry of cytoskeletal proteins, such as α-actinin, and the formation of a vinculin-rich focal adhesion-like complex are also dependent upon IpaA (Tran Van Nhieu *et al*., 1997). As IpaA binds directly to vinculin (Tran Van Nhieu *et al*., 1997), a component of adhesion structures, IpaA, was proposed to control cytoskeletal rearrangements through vinculin.

Vinculin is a cytoskeletal protein present at cell–cell and cell–matrix adhesion structures, implicated in a number of processes including cell motility, cell attachment to the substrate (Ezzell *et al*., 1997) and tumorigenesis (Rodriguez Fernandez *et al*., 1992). Vinculin consists of two domains: a compact globular N-terminal head domain

connected by a flexible proline-rich hinge to a rod-like C-terminal tail domain (Molony and Burridge, 1985). A number of structural studies have put forward vinculin as a key regulator of the cytoskeleton. For example, talin and α-actinin bind to the N-terminal domain of vinculin (Otto, 1983; McGregor *et al*., 1994), whereas an F-actin-binding site has been identified in the C-terminal tail (Menkel *et al*., 1994). These interactions are regulated by vinculin conformation. In its folded conformation, the tail domain interacts with the head domain and most vinculin ligand-binding sites are masked (Jockusch and Rüdiger, 1996). In its opened conformation, the intramolecular association between the head and the tail domains is disrupted and ligand-binding sites are exposed. Upon activation, vinculin unfolds and, by binding to talin or α-actinin via its head domain and to F-actin via its tail domain, acts as a linker between the cell membrane and the cytoskeleton (Johnson and Craig, 1994, 1995; Kroemker *et al*., 1994). The molecular mechanisms that lead to vinculin activation are not well understood. Binding of the signaling molecule phosphatidylinositol-4,5 bisphosphate (PIP_2) to vinculin has been shown to lead to unfolding of vinculin (Gilmore and Burridge, 1996; Hüttelmaier *et al*., 1998) but, because there are two PIP_2-binding sites located on the tail domain of vinculin (Tempel *et al*., 1995), PIP_2 could also potentially interfere with the association of vinculin with F-actin (Steimle *et al*., 1999).

To define further the role of the association between IpaA and vinculin, we characterized the IpaA-binding site on vinculin. In this study, we showed that IpaA acts as a potent activator of vinculin and increases the ability of vinculin to interact with F-actin. We also demonstrated that the vinculin–IpaA complex has depolymerizing activity on actin filaments, both *in vitro* and in microinjected cells, an activity that may help to explain some aspects of the IpaA-mediated modulation of the bacterial entry focus.

Results

IpaA binds to the first 265 N-terminal residues of vinculin

Vinculin overlay assays were used to define the IpaA-binding domain on vinculin. For this purpose, vinculin was obtained from chicken gizzards after purification on anion exchange chromatography as previously described (Evans *et al*., 1984). The N-terminal head domain of vinculin, corresponding to residues 1–850, as well as the C-terminal tail domain (residues 857–1066) were isolated after cleavage of full-length vinculin by the *Staphylococcus aureus* V8 protease (Figure 1A). The head domain of vinculin was then tested for its capacity to bind to IpaA in overlay assays. As shown previously, full-length vinculin specifically interacted with IpaA (Figure 1B, vinculin) and showed no significant binding to other *Shigella* proteins present in the extracts (Tran Van Nhieu *et al*., 1997). When the vinculin head domain was used as a probe, a strong signal was observed at the place of IpaA migration in a Western blot of extracts from wild-type *Shigella* (Figure 1B, head, wt), but not in extracts from an *ipaA* mutant (Figure 1B, head, A^-). These results indicated that the head domain of vinculin specifically bound to IpaA. When tested in similar assays, the vinculin tail domain did not show detectable binding to IpaA (data not shown).

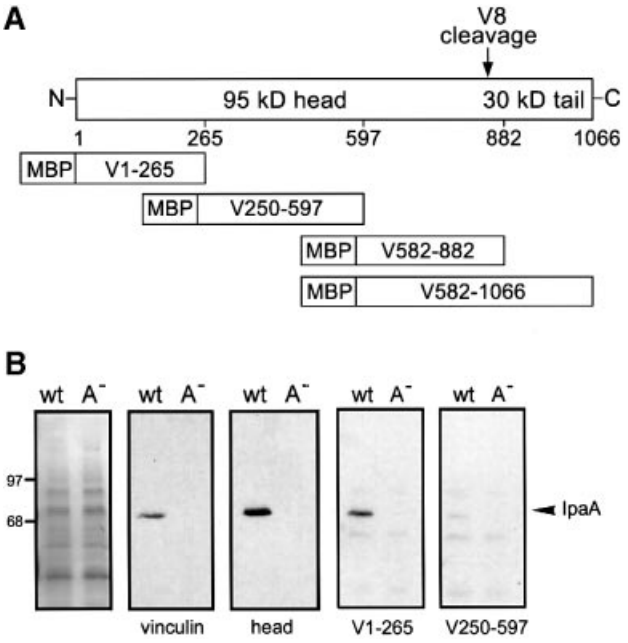

Fig. 1. IpaA binds to the first 265 N-terminal residues of vinculin. (**A**) Schematic representation of vinculin and derivatives. The 95 kDa vinculin head domain is separated from the 30 kDa vinculin tail domain by a *S.aureus* V8 protease cleavage site. Four MBP fusion proteins, containing vinculin residues 1–265 ($MBPV_{1–265}$), 250–597 ($MBPV_{250–597}$), 582–882 ($MBPV_{582–882}$) and 882–1066 ($MBPV_{882–1066}$) were generated. The numbers refer to the amino acid positions on vinculin. (**B**) IpaA binds to the N-terminal 1–265 residues of vinculin. Gel overlay assays were conducted using whole bacterial extracts of wild-type *Shigella* M90T (wt) or *ipaA* mutant (A^-). Extracts were separated by SDS–PAGE and stained with Coomassie Blue (left panel) or transferred to a filter. Filter replicas were probed with full-length vinculin (vinculin), the vinculin head domain (head) or the MBP fusion proteins $MBPV_{1–265}$ (V1–265) or $MBPV_{250–597}$ (V250–597). Protein binding was detected by immunoblotting using the anti-vinculin monoclonal antibody VIN 11.5 to detect binding of vinculin or the vinculin head, or using anti-MBP antiserum to detect binding of MBP–vinculin fusions. The molecular weight markers are indicated. Both vinculin and the head domain bind to IpaA (arrow). The $MBPV_{1–265}$ fusion protein, but not the $MBPV_{250–597}$ fusion protein, binds to IpaA.

To determine further which domain of the vinculin head was implicated in IpaA binding, four DNA fragments encompassing the entire vinculin cDNA and encoding residues 1–265, 250–597, 582–882 and 582–1066 (Figure 1A) were produced by PCR and cloned in the pMAL-p2 vector (Materials and methods). Maltose-binding protein (MBP)–vinculin fusion proteins were purified from *Escherichia coli* transformants by affinity chromatography. The purified fusion proteins were tested for their capacity to bind to IpaA in overlay assays, and protein binding was detected using anti-MBP antiserum. The $MBPV_{1–265}$ construct was the only protein found to interact with IpaA (Figure 1B, V1–265). The three other MBP–vinculin constructs did not show significant binding to IpaA (Figure 1B, V250–597 and data not shown), even when higher probing concentrations were used.

To characterize binding of IpaA to vinculin further, we developed a solid-phase assay in which IpaA, expressed as a GST fusion protein, was coated onto plastic wells. Vinculin was incubated with GST–IpaA-coated wells at

concentrations ranging from 0.5 to 100 nM, and vinculin binding was measured by an enzyme-based immunodetection procedure. As shown in Figure 2A, vinculin binding to IpaA was saturable, with maximal binding occurring at a concentration of ~7 nM, and with a dissociation constant (K_d) of 5 ± 0.1 nM after extrapolation from the Lineweaver–Burke graph (inset in Figure 2A). To confirm that IpaA binds to the first 265 N-terminal residues of vinculin, the $MBPV_{1–265}$ fusion protein was tested for its ability to compete with full-length vinculin for IpaA binding. Vinculin was incubated in GST–IpaA-coated wells in the presence of increasing concentrations of the $MBPV_{1–265}$ fusion. Binding of vinculin to IpaA was inhibited by the $MBPV_{1–265}$ fusion (Figure 2B, empty squares) with a half-maximum inhibitory concentration of 2.5 nM. In contrast, the $MBPV_{250–597}$ fusion did not interfere with vinculin binding to IpaA (Figure 2B, solid circles).

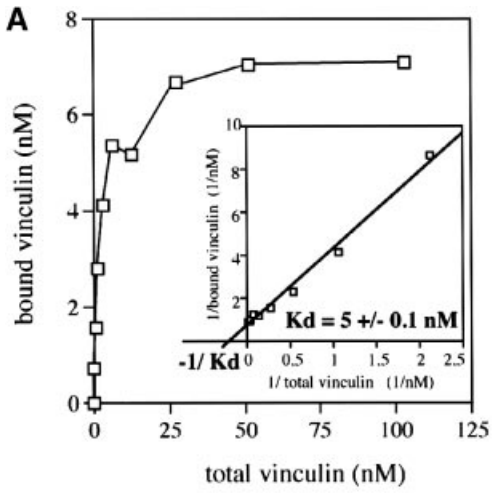

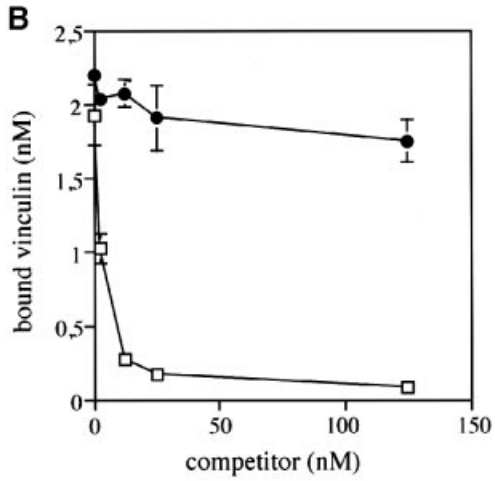

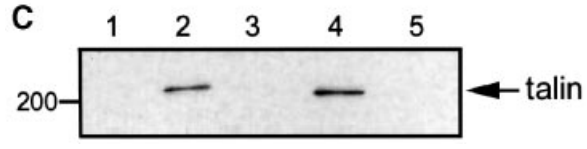

To substantiate these findings further, the interaction between IpaA and vinculin was probed in the yeast two-hybrid system. As in our other assays, a strong interaction between the vinculin head domain and IpaA was found, independently of whether *ipaA* was cloned in the DNA-binding or the activation domain vector. Using vinculin head deletion constructs, we could then show that the IpaA-binding site is confined to vinculin residues 1–258, whereas a fragment comprising vinculin residues 259–850 did not show any interaction with IpaA. β-Galactosidase activity determination assays indicated that the vinculin 1–258–IpaA interaction was slightly stronger (1.2-fold) than the vinculin head–tail interaction, which has been reported to have a K_d in the nanomolar range (Johnson and Craig, 1994). Thus, our two-hybrid data are in full accordance with our biochemical data.

Talin, a focal adhesion protein, binds to the first 258 amino acids of vinculin (Gilmore *et al*., 1993). To demonstrate a potential interference between talin and IpaA for binding to vinculin, co-immunoprecipitation experiments were performed. Talin was incubated with vinculin in the absence or presence of IpaA. Vinculin and vinculin-associated proteins were then pelleted after incubation with beads coated with anti-vinculin antibodies, and proteins associated with the beads were analyzed by Western blotting with an anti-talin monoclonal antibody. As shown in Figure 2, talin co-immunoprecipitated with vinculin (Figure 2C, lane 2). A stronger signal was observed when the head domain of vinculin was used instead of full-length vinculin (Figure 2C, lane 4), in agreement with previous studies (Johnson and Craig, 1994). When IpaA was added, however, talin did not associate with vinculin (Figure 2C, lane 3). These results indicate that IpaA interferes with the binding of talin to vinculin, consistent with the binding domain of IpaA being located between residues 1 and 265 on vinculin.

Fig. 2. Binding of IpaA to vinculin in a solid-phase assay and competition experiments. (**A**) Vinculin displays high affinity for IpaA. Microtiter wells were coated with the GST–IpaA fusion protein at a final concentration of 2 μg/ml. Vinculin was added to the wells at concentrations ranging from 0.5 to 100 nM, and vinculin binding was detected with the VIN 11.5 monoclonal antibody followed by enzyme-linked detection procedures. Each value represents the mean of three determinations. The dissociation constant (K_d) of the vinculin–IpaA interaction was extrapolated from the Lineweaver–Burke representation (inset): $K_d = 5 \pm 0.1$ nM. (**B**) Vinculin binding to IpaA is inhibited by $MBPV_{1–265}$. Microtiter wells were coated as in (A). Vinculin was added to the wells at a constant concentration of 2.5 nM, with increasing amounts of $MBPV_{1–265}$ (□) or $MBPV_{250–597}$ (o). Detection of vinculin binding was monitored using the anti-vinculin VIN 11.5 monoclonal antibody. Specific binding of vinculin was determined as the values obtained for vinculin binding to GST–IpaA-coated wells, from which the values for binding to BSA-coated wells were subtracted. Each experiment was performed in triplicate. $MBPV_{1–265}$ but not $MBPV_{250–597}$ competes with vinculin for IpaA binding. (**C**) IpaA inhibits talin binding to vinculin. Vinculin was incubated with talin in the presence or absence of IpaA, and vinculin-associated proteins were recovered by immunoprecipitation using monoclonal antibodies against vinculin. Lane 1, vinculin alone; lane 2, talin and vinculin; lane 3, talin, vinculin and IpaA; lane 4, talin and the vinculin head domain; lane 5, talin alone. Samples were analyzed by Western blotting using anti-talin monoclonal antibody. Full-length talin is indicated by an arrow. The 200 kDa marker is indicated. Talin co-immunoprecipitates with full-length vinculin or with the vinculin head, but IpaA inhibits talin association with vinculin.

IpaA induces F-actin depolymerization in a vinculin-dependent manner

The interactions between vinculin and its ligands are regulated by vinculin conformational changes. In the folded conformation of vinculin, the head and the tail domains are held by intramolecular association. This prevents F-actin from binding to the tail domain of vinculin. In contrast, in its unfolded conformation, the F-actin-binding site of the vinculin tail domain is unmasked (Johnson and Craig, 1995). To determine the effects of IpaA on vinculin binding to F-actin, pelleting assays were conducted. Actin filaments were incubated either with vinculin alone or with vinculin in the presence of IpaA. After incubation, F-actin and F-actin-associated proteins were pelleted by ultracentrifugation. Pellet and supernatant fractions were analyzed by SDS–PAGE and stained with Coomassie Blue. In the absence of other proteins, ~80% of the actin pool polymerized and sedimented in the pellet (Figure 3A). No difference in this percentage was observed when IpaA alone or vinculin alone were incubated with F-actin prior to ultracentrifugation (Figure 3A). When vinculin at a concentration of 140 nM and IpaA were incubated together, however, actin was found predominantly in the supernatant fraction (Figure 3A). This indicates that IpaA was able to induce F-actin depolymerization in the presence of vinculin. When varying the concentration of vinculin using a constant concentration of IpaA, a direct correlation was observed between the extent of actin depolymerization and vinculin concentration (Figure 3A, 4, 18 and 140 nM). For a given concentration of vinculin (140 nM), actin was still unable to sediment even at very low concentrations of IpaA, with a similar efficiency for concentrations of IpaA between 5 and 20 nM (data not shown).

To determine whether the F-actin-binding site on vinculin was necessary for F-actin depolymerization mediated by the vinculin–IpaA complex, pelleting assays were conducted with the vinculin head domain, which lacks the actin-binding site. As shown in Figure 3B, no difference was observed in the amounts of actin recovered in the supernatant of samples incubated with IpaA and the vinculin head domain, IpaA alone or the head domain alone. This indicates that even though IpaA binds to the vinculin head (Figure 1B), IpaA does not promote depolymerization of actin filaments in the presence of the vinculin head domain. We conclude that the F-actin-binding site located on the vinculin tail is necessary for actin depolymerization induced by the vinculin–IpaA complex.

To analyze further the effects of the vinculin–IpaA complex on actin filaments, F-actin pre-treated with the vinculin–IpaA complex was analyzed by electron microscopy. As shown in Figure 3C, untreated F-actin organized into slack networks that covered the grid evenly. When actin filaments were incubated with vinculin and IpaA, the majority of actin filaments were no longer visible (Figure 3D), indicating that depolymerization had occurred. In some instances, tight bundles could be observed (Figure 3D, arrowhead), which appear to contain short actin filaments (data not shown).

IpaA stimulates vinculin binding to F-actin

Results from the previous section suggest that the interaction between F-actin and the vinculin–IpaA complex occurs via the tail domain of vinculin, and that the interaction between IpaA and vinculin results in unmasking of the F-actin-binding domain of the vinculin tail. The effects of IpaA on the conformation of vinculin were therefore investigated.

Actin filaments were stabilized with phallacidin to avoid depolymerization, and filaments were incubated with vinculin in the presence of IpaA. F-actin and F-actin-associated proteins were pelleted by ultracentrifugation.

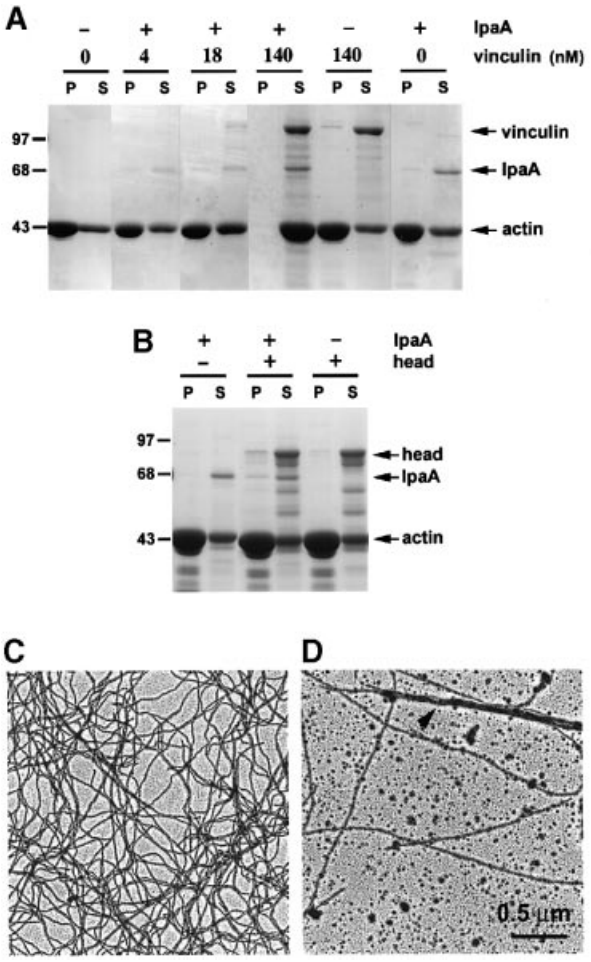

Fig. 3. The vinculin–IpaA complex induces F-actin depolymerization. (**A**) The vinculin–IpaA complex prevents actin sedimentation. Pelleting assays were performed at pH 7.0. F-actin was incubated for 2 h with vinculin at concentrations of 4, 18 or 140 nM in the absence (–) or presence (+) of IpaA, as indicated. F-actin-associated proteins were pelleted by ultracentrifugation. Pellet (P) and supernatant (S) fractions were analyzed by SDS–PAGE on a gel containing 10% polyacrylamide. Proteins were visualized by Coomassie Blue staining. Arrows indicate the position of vinculin, IpaA and actin. The 97, 68 and 43 kDa markers are indicated. (**B**) The complex formed by the vinculin head domain and IpaA does not affect F-actin solubility. Pelleting assays were conducted as in (A) by incubating F-actin in the presence (+) or absence (–) of IpaA and the vinculin head domain, as indicated. After centrifugation, pellet (P) and supernatant (S) fractions were analyzed by SDS–PAGE and stained with Coomassie Blue. Arrows indicate the position of the vinculin head domain, IpaA and actin. (**C** and **D**) Electron microscopy analysis of the effects of the vinculin–IpaA complex on F-actin. F-actin (3.5 μM) was incubated for 2 h either with buffer alone (C) or with vinculin (0.6 μM) and IpaA (0.1 μM) (D). Samples were applied on electron microscopy grids and were negatively stained with uranyl acetate and rotary shadowed. The vinculin–IpaA complex induces F-actin depolymerization, along with the occasional formation of actin filament bundles (arrowhead in D). Scale bar, 0.5 μm for (C) and (D).

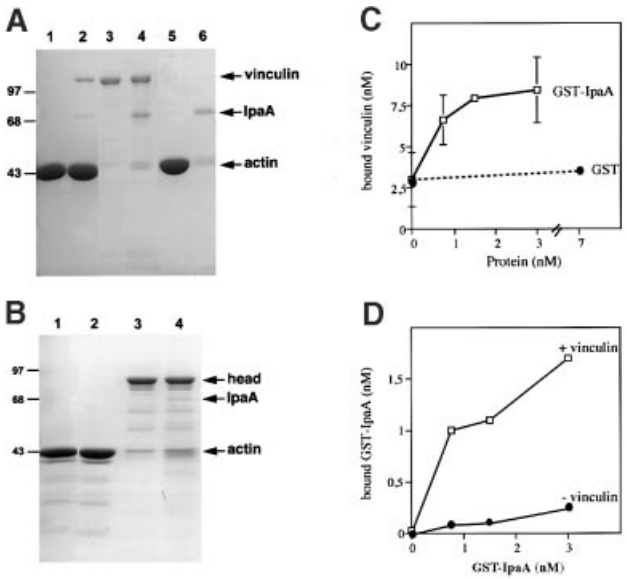

Fig. 4. IpaA induces vinculin binding to F-actin. (**A**) Vinculin binds to F-actin in the presence of IpaA in a co-sedimentation assay. F-actin (2 μM) was stabilized with phallacidin 2 h prior to incubation with either 130 nM vinculin (lanes 1 and 3), 130 nM vinculin and 30 nM IpaA (lanes 2 and 4) or 30 nM IpaA alone (lanes 5 and 6). Samples were subjected to ultracentrifugation, and supernatant (lanes 3, 4 and 6) and pellet (lanes 1, 2 and 5) fractions were analyzed by SDS–PAGE. Proteins were visualized by Coomassie Blue staining. Proteins are indicated with arrows. The 97, 68 and 43 kDa markers are indicated. (**B**) The vinculin head domain does not associate with F-actin in the presence of IpaA. F-actin stabilized with phallacidin was incubated with the vinculin head domain at 190 nM (lanes 1 and 3) or with the head domain (190 nM) and IpaA (30 nM) (lanes 2 and 4). Samples were subjected to ultracentrifugation, and pellet (lanes 1 and 2) and supernatant (lanes 3 and 4) fractions were analyzed by SDS–PAGE. Proteins were visualized by Coomassie Blue staining. Proteins are indicated with arrows. The 97, 68 and 43 kDa markers are indicated. (**C**) IpaA induces vinculin binding to immobilized F-actin. Microtiter wells were coated with F-actin at a concentration of 500 μg/ml. Vinculin was incubated at a constant concentration of 12 nM with immobilized F-actin in the presence of GST–IpaA at concentrations ranging from 0.8 to 3 nM (□) or in the presence of 7 nM GST (●). Vinculin binding was detected with the anti-vinculin VIN 11.5 monoclonal antibody. Each point represents the mean of three independent experiments, and the standard deviations are indicated. Each assay was conducted in triplicate. (**D**) IpaA does not bind to F-actin. Assays were carried out as in (C) except that an anti-IpaA monoclonal antibody was used to detect binding of GST–IpaA to wells coated with F-actin. GST–IpaA was added to wells at concentrations ranging from 0.8 to 3 nM in the presence (□) or absence of vinculin (●). Bound antibodies were detected as in (C). The graph shows results from a representative experiment where each determination was performed in duplicate.

As shown in Figure 4, in the absence of IpaA, no vinculin was detected in the pellet (Figure 4A, lane 1), indicating that vinculin alone could not interact significantly with F-actin. When IpaA was added, however, a significant fraction of vinculin bound to F-actin (Figure 4A, lane 2). IpaA alone did not bind to stabilized actin filaments (Figure 4A, lane 5) but, in the presence of vinculin, a significant fraction of IpaA associated with F-actin (Figure 4A, lane 2). These results suggest that association of the vinculin–IpaA complex with actin occurs via the F-actin-binding domain located on the tail of vinculin. Consistent with this, the vinculin head domain did not bind to F-actin in the presence of IpaA (Figure 4B, lane 2).

A solid-phase assay was developed to measure the effects of IpaA on the association between vinculin and F-actin. Actin filaments were coated onto plastic wells and vinculin was added to immobilized F-actin in the presence or absence of a GST–IpaA fusion protein. Bound proteins were detected using immunodetection methods. Consistent with data from F-actin co-sedimentation assays, vinculin alone bound poorly to F-actin, with 20% of the total pool of vinculin binding to immobilized F-actin (Figure 4C). In the presence of GST–IpaA, however, vinculin binding to immobilized F-actin was increased dramatically. Concentrations of GST–IpaA as low as 3 nM increased the association between vinculin and F-actin by 3-fold (Figure 4C, empty squares). In control experiments, addition of GST had no effect on vinculin activation (Figure 4C, solid circles), and GST–IpaA by itself showed little binding to F-actin (Figure 4D, solid circles). Association of GST–IpaA with F-actin was only detected when vinculin was added (Figure 4D, empty squares).

Taken together, both co-sedimentation experiments and solid-phase assays indicate that IpaA stimulates the association of vinculin with F-actin. This strongly suggests that IpaA interaction with vinculin unmasks the F-actin-binding site on the vinculin tail.

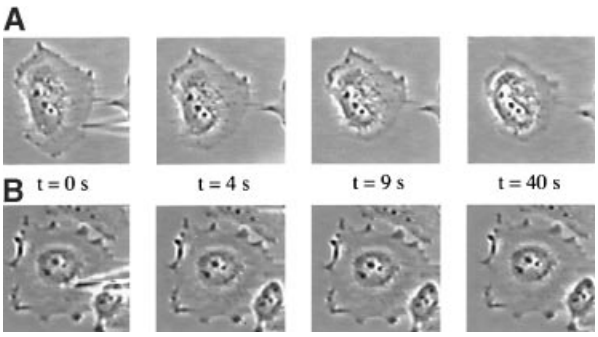

Fig. 5. Microinjection of IpaA into HeLa cells induces cell retraction. Samples were microinjected into HeLa cells and the effects on the cell morphology were analyzed by phase-contrast videomicroscopy. Images were captured before microinjection (t = 0 s), or at 4, 9 or 40 s following microinjection (t = 4 s, t = 9 s, t = 40 s). Retraction of the cell was observed within 40 s following microinjection. (**A**) IpaA at a concentration of 20 ng/μl and FITC–dextran. (**B**) FITC–dextran alone.

Microinjection of IpaA in cultured cells induces the disappearance of actin stress fibers

To study its effects on the cytoskeleton, IpaA was microinjected into HeLa cells. HeLa cells were plated on glass coverslips and grown for 24 h prior to microinjection. The effects of IpaA microinjection on the cell morphology were analyzed by phase-contrast videomicroscopy. As shown in Figure 5, microinjection of IpaA led to rapid cell retraction. Retraction occurred within the first 40 s following microinjection and resulted in the loss of up to 40% of initial cell spreading surface (Figure 5A). Few morphological changes were observed following this rapid retraction phase. No significant rearrangements were observed in control cells that were microinjected with fluorescein isothiocyanate (FITC)–dextran alone (Figure 5B).

To characterize cytoskeletal rearrangements induced by IpaA, cells were microinjected with IpaA and incubated at 37°C for 5 min. Samples were then fixed and processed for fluorescence staining of F-actin or vinculin. The data

presented in Figure 6 are representative of at least 100 microinjected cells analyzed for each sample in at least two independent experiments. In the absence of microinjection, cells typically were well spread and showed numerous and well-defined stress fibers. Microinjection of the FITC–dextran marker did not lead to significant changes in actin organization (Figure 6A). In contrast, when IpaA was microinjected, disruption of the stress fiber network and retraction fibers were observed (Figure 6B and C). Two characteristic phenotypes could be associated with microinjection of IpaA. In 52% of microinjected cells, stress fibers disappeared and short actin cables were visible with radial reorientation from the perinuclear region to the cell edges (Figure 6B and G, IpaA, gray bar). Other microinjected cells showed a significant decrease in the number of actin cables, with thinner actin filaments localizing, for the most part, at the cell periphery (Figure 6C). This was accompanied by disruption of the subcortical actin belt resulting in less defined cell contours (Figure 6C). Such depolymerization occurred in 31% of microinjected cells (Figure 6G, IpaA, solid bar). These cell phenotypes were observed with the same frequency when cells were incubated for 15 min at 37°C after microinjection (data not shown).

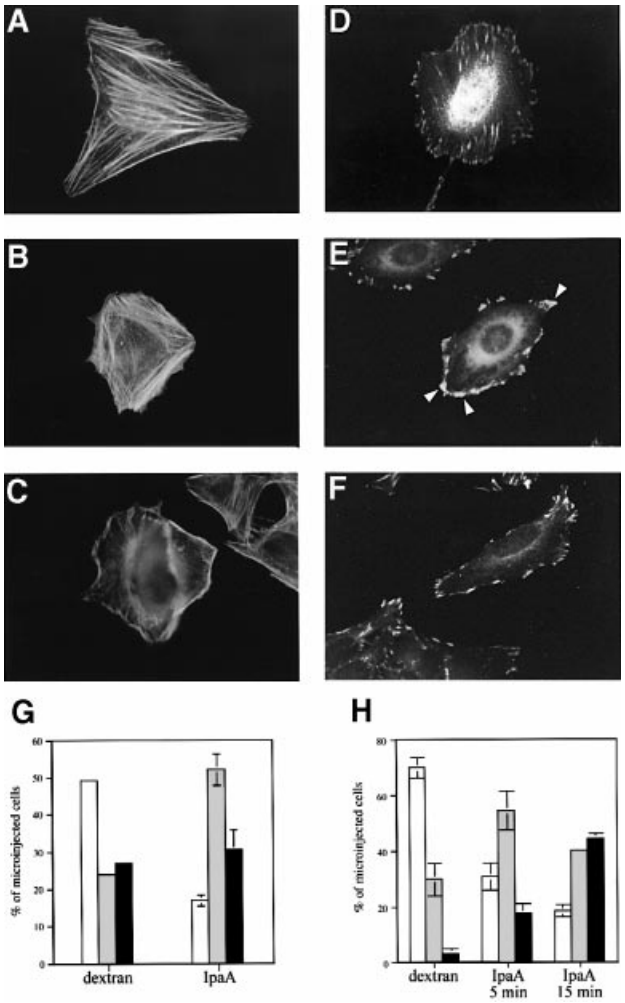

Fig. 6. Cytoskeletal rearrangements in HeLa cells microinjected with IpaA. Following microinjection with either FITC–dextran (**A** and **D**) or IpaA (**B**, **C**, **E** and **F**), HeLa cells were incubated for 5 min at 37°C, fixed and permeabilized. Cells were stained with rhodamine–phalloidin (A–C), or the anti-vinculin hvin1 antibody and anti-mouse rhodamine–IgG (D–F). IpaA microinjection resulted in cell retraction with short actin cables located in the perinuclear region and radially from the nucleus to the cell edges (B), or in the disappearance of actin cables (C). Clusters of vinculin-rich focal complexes are shown with arrowheads (E). (**G**) F-actin rearrangements induced by IpaA. Microinjected cells were classified into three categories: cells with no significant changes as in (A) (empty bars); cells presenting short actin cables as in (B) (gray bars); or cells with a loss of actin cables as in (C) (solid bars). An average of 100 microinjected cells in two independent experiments was scored for each sample. Standard deviations are indicated. Dextran, cells microinjected with FITC–dextran and incubated for 5 min at 37°C before fixation; IpaA, cells microinjected with IpaA and FITC–dextran and incubated for 5 min at 37°C before fixation. (**H**) Vinculin-rich focal complex rearrangements induced by IpaA. Microinjected cells were divided into three categories: cells with no significant changes as in (D) (empty bars); cells presenting clusters of focal complexes at the periphery as in (E) (gray bars); and cells displaying a disappearance of focal adhesions as in (F) (solid bars). Dextran, cells microinjected with FITC–dextran; IpaA 5 min, cells microinjected with IpaA and FITC–dextran and incubated for 5 min at 37°C before fixation; IpaA 15 min, cells microinjected with IpaA and FITC–dextran and incubated for 15 min at 37°C before fixation.

When stained with anti-vinculin antibody, cells typically showed numerous focal adhesions located at the periphery and at the inner basal surface of the cell, and microinjection with FITC–dextran alone did not promote any significant changes in the number or organization of focal adhesions (Figure 6D). Shortly after IpaA microinjection, however, the large focal adhesions located at the inner basal surface of the cell disappeared (Figure 6E). Instead, large vinculin-rich patches appeared at the cell edges, suggesting a clustering of focal complexes at the cell periphery (Figure 6E, arrows). This effect was observed in 53% of the microinjected cells (Figure 6H, IpaA 5 min, gray bar), as early as after 5 min of incubation following microinjection. Upon incubation at 37°C, an increasing number of microinjected cells showed a decrease of vinculin-containing focal complexes (Figure 6F), with 45% of microinjected cells showing total disappearance of vinculin patches after 15 min incubation (Figure 6H, IpaA 15 min, solid bar).

When IpaA was co-microinjected with the $MBPV_{1–265}$ fusion, cell retraction induced by IpaA was inhibited and stress fibers and vinculin-containing focal complexes could still be observed, whereas no significant change in the IpaA effect was observed when IpaA was co-microinjected with the $MBPV_{250–597}$ fusion (data not shown). These results indicate that the vinculin–IpaA binding domain interferes with IpaA-induced cytoskeletal rearrangements.

Discussion

IpaA induces vinculin binding to F-actin

Using co-sedimentation and solid-phase assays, we have shown that the association between vinculin and F-actin is strongly increased in the presence of IpaA. Association of the vinculin–IpaA complex with F-actin certainly occurs via the vinculin tail domain since neither IpaA alone nor IpaA complexed with the head domain of vinculin can interact with F-actin. This strongly suggests that IpaA unmasks the cryptic F-actin-binding site of the vinculin tail. To our knowledge, IpaA is the first example of a protein ligand that activates vinculin. Cellular ligands, such as talin and α-actinin, have been described to bind preferentially to the opened form of vinculin but they do

not have the ability to stimulate its ability to bind to F-actin (Johnson and Craig, 1994; Kroemker *et al*., 1994). We have shown that IpaA binds to a region encompassing the first 265 amino acids of vinculin. Interestingly, the 1–258 domain of vinculin has also been shown to be involved in the intramolecular association with the C-terminal tail domain (Jockusch and Rüdiger, 1996). It is therefore possible that mere binding of IpaA to this domain disrupts the head–tail interaction. The fact that talin, which binds to the same domain as IpaA, does not induce a significant increase in vinculin association with F-actin could be due to different affinities of talin and IpaA for vinculin. Consistent with this, we have shown that IpaA binds to vinculin with a K_d of 5 nM, whereas similar assays indicated that talin interacts with vinculin with a K_d of 200–600 nM (Gilmore *et al*., 1993). High affinity binding of IpaA may stabilize a conformation of vinculin in which the F-actin-binding domain located on the vinculin tail remains freely accessible.

Actin depolymerization induced by the vinculin–IpaA complex

The vinculin–IpaA complex was found to promote F-actin depolymerization. In contrast, a complex consisting of IpaA associated with the N-terminal head domain of vinculin was not able to depolymerize F-actin. Since neither IpaA alone nor IpaA associated with the vinculin head domain bind to F-actin, we propose that the vinculin tail domain provides the link between IpaA and F-actin, and that actin depolymerization requires prior conformational change of vinculin induced by IpaA. The observation that depolymerization is dependent on vinculin concentration supports the notion that vinculin is a limiting factor for the depolymerization process. There are two major subclasses of actin-depolymerizing factors, the gelsolin and the ADF/cofilin families. The severing activity of these proteins on actin filaments is modulated by various conditions including pH and calcium (Hayden *et al*., 1993; Lamb *et al*., 1993). In addition to depolymerization, ADF/cofilin and gelsolin have been shown to co-sediment with actin filaments, to bind to monomeric actin and to favor nucleation of actin filaments. This has raised controversy on the exact role of these factors in F-actin regulation, and on the regulation of these different activities in the cell. In contrast to ADF/cofilin or gelsolin, maximal depolymerization induced by the vinculin–IpaA complex occurred between pH 7.0 and 7.5. Under more acidic or more basic conditions, for pH $<$6.5 and pH $>$8.0, very little depolymerization activity could be detected, and the vinculin–IpaA complex exhibited exclusively an F-actin-binding property (R.Bourdet-Sicard, unpublished data). As expected, electron microscopic analysis revealed that the vinculin–IpaA complex induced a disappearance of the actin filament network. Interestingly, a few actin bundles were observed together with the disappearance of filaments. These bundles could result from a bundling activity associated with vinculin activation by IpaA. The vinculin tail domain has been shown to cross-link F-actin at a stoichiometric ratio and to bundle actin filaments when used at higher stoichiometry (Korneeva and Jockusch, 1996; Hüttelmaier *et al*., 1997; Rüdiger *et al*., 1998). These activities could be determined by the two F-actin-binding sites on the vinculin tail and/or the ability of tail domains to form oligomers.

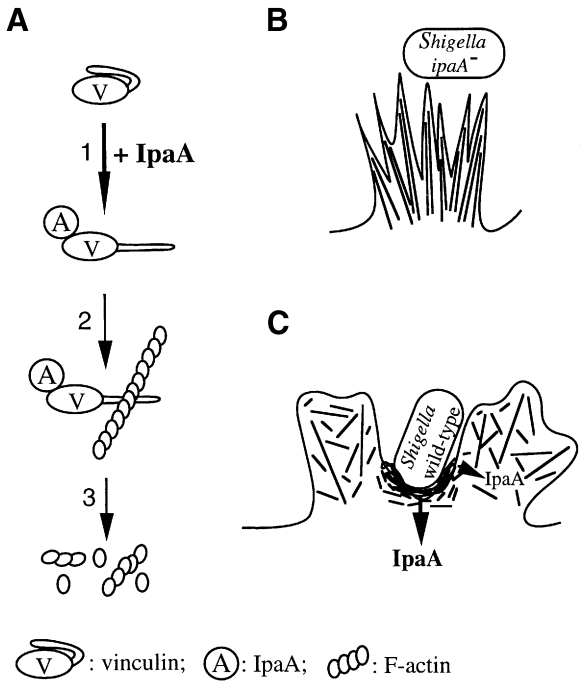

Fig. 7. Effect of the vinculin–IpaA complex on F-actin and roles in cytoskeletal rearrangement during *Shigella* entry. (**A**) IpaA binds to vinculin and leads to a conformational change of vinculin (arrow 1). The vinculin–IpaA complex associates with actin filaments via the F-actin-binding site on the vinculin tail (arrow 2) and induces actin depolymerization (arrow 3). (**B**) Numerous microspikes, due to massive uncontrolled actin polymerization, are formed and *Shigella ipaA* mutant (*ipaA*$^-$) is repelled from the cell surface. (**C**) Depolymerization induced by the vinculin–IpaA complex leads to the formation of a network of short actin filaments at the site of bacterial–cell contact, and modulates the formation of cell extensions surrounding the wild-type bacterium. A gradient in IpaA concentration could account for total or only partial F-actin depolymerization.

Role of the vinculin–IpaA complex in the Shigella entry process

Shigella and *Salmonella* enter into cells by a 'trigger' mechanism associated with large cellular deformations, whereas other pathogens such as *Listeria* or *Yersinia* enter into cells by a 'zipper' mechanism involving limited membrane deformations. In the case of the zipper mechanism, bacteria bind tightly to cell surface receptors. Although associations between the adhesion molecule CD44 and the IpaB invasin (A.Skoudy, J.Mounier, A.Aruffo, H.Ohayon, P.Gounon, P.Sansonetti, G.Tran Van Nhieu, submitted) or between the $\alpha_5\beta_1$ integrin and the IpaB–C complex (Watarai *et al*., 1996) have been described for *Shigella*, these interactions do not promote strong bacterial adhesion. Upon translocation in the cell cytosol and association with vinculin, IpaA potentiates bacterial entry and modulates *Shigella*-induced cytoskeletal rearrangements (Tran Van Nhieu *et al*., 1997). In Figure 7, we propose a model that converges features linked to IpaA during *Shigella*-induced foci formation, and vinculin activation and actin depolymerization induced by IpaA, reported in this study. IpaA binds to vinculin and unfolds it (Figure 7A, arrow 1). The vinculin–IpaA complex could then interact with actin filaments (Figure 7A, arrow 2)

and depolymerize them (Figure 7A, arrow 3). We propose that the vinculin–IpaA complex, through actin depolymerization, regulates the formation of projections that would otherwise repel the bacterium from the cell surface, as observed in the case of the *Shigella ipaA* mutant (Figure 7B). Also, activation of vinculin by IpaA at this level could allow the recruitment of focal adhesion components, which leads to the formation of a specific focal adhesion-like structure, strengthening bacterial adhesion to the cell surface. The vinculin–IpaA complex could recruit α-actinin since IpaA and α-actinin binding on vinculin are not mutually exclusive (R.Bourdet-Sicard, unpublished data). Cross-linking of short actin filaments promoted by plastin or α-actinin and severing of actin filaments by the vinculin–IpaA complex could account for the transition of microspikes into leaflets, observed in entry foci induced by the wild-type *Shigella* (Figure 7C). Finally, recruitment of cytoskeletal proteins induced by IpaA at the site of *Shigella* entry may lead to the recruitment of signaling molecules, such as tyrosine kinases, postulated to play a role in the down-modulation of foci of actin polymerization (G.Dumenie, P.Sansonetti, G.Tran Van Nhieu, submitted), and that is not observed in actin foci induced by a *Shigella ipaA* mutant (Tran Van Nhieu *et al*., 1997).

Materials and methods

Bacterial strains and plasmid constructs

Wild-type *S.flexneri* serotype 5 M90T was used in this study (Sansonetti *et al*., 1982). The *ipaA* mutant strain was obtained by plasmid insertion in the *ipaA* gene as previously described (Ménard *et al*., 1993). The *ipaB* mutant strain, which constitutively secretes the Ipa proteins, was kindly provided by Dr Claude Parsot (Ménard *et al*., 1993). Bacterial strains were grown in trypticase soy broth (BTCS) (BBL) at 37°C with constant agitation.

To obtain the GST–IpaA fusion, a 2.2 kb *Nsi*I–*Pvu*II fragment corresponding to the entire *ipaA* coding sequence deleted from its first two N-terminal residues was cloned in the *Sma*I site of plasmid pGEX-2T (Pharmacia Biotech) after blunt-end ligation.

To generate MBP–vinculin peptides, vinculin DNA fragments were obtained by PCR using the plasmid pJ4Ω:vinc (Rodriguez Fernandez *et al*., 1992) as a template. PCR products were generated either with *Eco*RI or *Hin*dIII sites at both ends and a stop codon at the 3′ end for the fragments encoding amino acids 1–265 and 582–1066 of vinculin, or with *Sal*I or *Not*I sites for the fragments encoding amino acids 250–597 and 582–882 of vinculin. The primers used for PCR were 5′-CACTGAATTCATGCCCGTCTTCCAC-3′ and 5′-AGGCAAGCTTTCACATGGCTTCAGTGTCCTTGCT-3′ for the fragment 1–265; 5′-CGCCGAATTCAAAGCACGGATGCAA-3′ and 5′-CCGGAAGCTTTTACTGATACCATGGGGGTC-3′ for the fragment 582–1066; 5′-ATCGGTCGACCTCACTTCCTGGGAT-3′ and 5′-TATAGCGGCCGCATCAGACACCTCCTG-3′ for the fragment 250–597; and 5′-AATGGTCGACGATCTCAAAGCACGG-3′ and 5′-ATATGCGGCCGCTGGGAACTCCTCATC-3′ for the fragment 582–882. For fragments 1–265 and 582–1066, PCR products were cleaved by *Eco*RI–*Hin*dIII (New England Biolabs) and inserted in the corresponding sites of pMAL-p_2 (New England Biolabs). For fragments 250–597 and 582–882, PCR products were cleaved by *Sal*I–*Not*I (New England Biolabs) and cloned into the *Hin*dIII site of pMAL-p_2 after blunt-end conversion. For each construct, cloning was checked by sequencing the fusion site between the *malE* gene and the vinculin DNA insert and, for the $MBPV_{1–265}$ construct, the entire insert was sequenced.

Purification of proteins

Vinculin was purified from chicken gizzards as described by Evans *et al*. (1984), with a few modifications. F-actin and several actin-associated proteins were cleared by precipitation with 10 mM $MgCl_2$, and the supernatant was precipitated with ammonium sulfate. After dialysis, vinculin extract was transferred onto a DEAE–Sephacel column (Pharmacia) and eluted using a 20–370 mM NaCl linear gradient. Vinculin-containing fractions were pooled and loaded onto a MonoQ FPLC column (Pharmacia) and fractions were eluted using a 10–300 mM NaCl linear gradient. Vinculin typically eluted as a homogeneous fraction at 200 mM NaCl. The head and tail domains of vinculin were obtained after proteolytic cleavage with the V8 protease of *S.aureus* (Sigma). The V8 protease was used at a final concentration of 5 μg/ml and incubated for 1 h at 37°C with 0.3 mg/ml vinculin in 25 mM Tris pH 7.6, 20 mM sodium acetate, 250 mM NaCl, 1 mM EGTA, 0.1 mM EDTA, 0.02% NaN_3. Products from proteolytic cleavage were dialyzed against 20 mM Tris pH 7.5, 20 mM NaCl containing 1 mM phenylmethylsulfonyl fluoride (PMSF) and loaded onto a MonoQ FPLC column (Pharmacia). The head domain was eluted using a 20–370 mM NaCl salt gradient. Talin was purified as previously described (Molony *et al*., 1987). The GST–IpaA fusion protein was purified according to the manufacturer's instructions (Pharmacia). MBP fusion proteins were purified from single transformants according to the manufacturer's instructions (New England Biolabs). IpaA was purified from the culture medium of an *ipaB Shigella* strain that constitutively secretes Ipa proteins (Ménard *et al*., 1993). Bacteria were grown in BTCS medium until the OD_{600} reached 1.8 U. Bacteria were harvested by centrifugation at 4000 *g* at 4°C for 15 min and the supernatant was transferred on ice. Proteins were concentrated by precipitation with ammonium sulfate at 60% final concentration. Proteins were resuspended in buffer A (20 mM Tris pH 7.0, 20 mM NaCl, 0.1 mM EDTA, 1 mM AEBSF and 0.1% NP-40) and dialyzed extensively against buffer A. The extract was loaded onto a MonoQ FPLC column (Pharmacia). Elution was performed using a linear gradient (20–500 mM NaCl). IpaA was eluted as a homogeneous fraction at 80 mM NaCl and was stored as aliquots at 400 nM at –80°C. Samples were thawed freshly before use.

Overlay assay

Vinculin overlay assays were performed as described (Otto, 1983) and vinculin binding was visualized using immunodetection procedures. Bacterial extracts were prepared as follows: bacteria were grown until early exponential phase (OD_{600} = 0.2) and samples were centrifuged at 3000 *g* for 5 min. Bacterial pellets were resuspended in one-tenth of the initial volume of Laemmli sample buffer (Laemmli, 1970) without reducing agent. Proteins were subjected to SDS–PAGE on a gel containing 10% polyacrylamide and transferred onto an Immobilon-P filter (Millipore). Filters were blocked in phosphate-buffered saline (PBS) containing 1% bovine serum albumin (BSA) (Sigma) and probed with full-length vinculin or vinculin-related peptides at a final concentration of 1 μg protein/ml in PBS containing 0.1% Tween-20 (PBS-T) (Sigma) for 1 h at room temperature, with gentle agitation. Filters were washed three times in PBS-T and incubated with the anti-vinculin monoclonal antibody VIN 11.5 (Sigma) at a final concentration of 100 ng/ml in PBS-T for 60 min, or with anti-MBP antiserum (New England Biolabs) to detect binding of MBP fusion proteins. Bound antibodies were detected by incubation with anti-mouse IgG or anti-rabbit IgG coupled to horseradish peroxidase (HRP) (Amersham or Nordic Immunology, respectively). After washing, bound proteins were detected using the ECL system (Amersham).

Solid-phase assay

To study the effects of IpaA on vinculin binding to F-actin, G-actin at 1 mg/ml (Cytoskeleton) was polymerized by adding salts at a final concentration of 100 mM KCl and 2 mM $MgCl_2$ and incubated at room temperature for 1 h. Then 96-well plates (NUNC-immunoplate maxiSorp, InterMed) were coated overnight at 4°C with 500 μg/ml F-actin. Wells were blocked in PBS containing 2% BSA for an additional 24 h. After washes with PBS-T, vinculin was added in the wells at a concentration of 12 nM in the presence of GST–IpaA at concentrations ranging from 0.8 to 3 nM. To study binding of IpaA to vinculin, microtiter wells were coated with 2 μg/ml GST–IpaA. Wells were blocked in PBS containing 2% BSA, and incubated with vinculin at concentrations ranging from 0.5 to 100 nM in PBS-T containing 2% BSA. To study the effects of MBP–vinculin fusion proteins on binding of vinculin to IpaA, vinculin was added to GST–IpaA-coated wells at a constant concentration of 2.5 nM. Bound vinculin was detected with the anti-vinculin VIN 11.5 monoclonal antibody (Sigma) that does not recognize $MBPV_{1–265}$ and $MBPV_{250–597}$. Bound GST–IpaA was detected using anti-IpaA monoclonal antibody (kind gift from Dr Kirsten Niebuhr). Bound antibodies were detected using anti-mouse HRP-labeled anti-IgG antibodies using the colorimetric substrate *o*-phenylenediamine dihydrochloride (OPD) (Sigma) and monitoring the absorbance at 490 nm with a microplate reader (Dynatech MR 4000). The concentration of reagents

was calibrated to allow reading of the absorbance under a linear range of detection.

Yeast two-hybrid assay

cDNAs for the vinculin head (VH; residues 1–850), the vinculin tail (VT; residues 858–1066) and truncated versions of VH (residues 1–258 and 259–850) were cloned into both the yeast two-hybrid activation domain vector pGAD424 (Clontech) and the DNA-binding domain vector pGBT9 (Clontech) as described earlier (Rüdiger *et al*., 1998). A cDNA fragment coding for IpaA was similarly cloned into the *Eco*RI–*Bam*HI site of both vectors. All yeast manipulations and color reactions on plates or in solution [ONPG (*o*-nitrophenyl-galactoside) assay] for semi-quantitative analysis of two-hybrid interactions were performed according to standard procedures and the manufacturer's protocols (Clontech).

Co-immunoprecipitation

For co-immunoprecipitation studies, 30 pmol of vinculin or 80 pmol of vinculin head domain was incubated with 15 pmol of talin overnight at 4°C in TEEAN buffer (10 mM Tris–HCl pH 7.5, 1 mM EGTA, 0.1 mM EDTA, 150 mM NaCl, 0.5 mM β-mercaptoethanol and 0.02% NaN_3) containing 1% BSA in the presence of 10 pmol of IpaA when indicated. Vinculin complexes were immunoprecipitated using the anti-vinculin monoclonal antibodies VIN 11.5 (Sigma) and hvin1 (Sigma) bound to protein G–Sepharose beads (Pharmacia) in TEEAN–1% BSA. Immunoprecipitated proteins were analyzed by Western blotting using an anti-talin monoclonal antibody (Sigma). Bound proteins were detected using anti-mouse IgG antibody linked to HRP and the ECL system (Amersham).
F-actin pelleting assays

Actin polymerization was induced by adding salts to a final concentration of 100 mM KCl and 2 mM $MgCl_2$ into a G-actin preparation (Cytoskeleton) at 1 mg/ml and incubated at room temperature for 1 h. When needed, phallacidin (Sigma) was added at a final concentration of 1.2 μM to stabilize F-actin. Proteins were added to F-actin in polycarbonate tubes (Beckman) and incubated for 2 h at room temperature in F-buffer (2 mM Tris–HCl pH 7.5, 0.2 mM $CaCl_2$, 0.5 mM β-mercaptoethanol, 0.2 mM ATP, 100 mM KCl and 2 mM $MgCl_2$). Proteins were centrifuged at 110 000 *g* for 30 min at 4°C in a TL100 ultracentrifuge (Beckman). Supernatant fractions were precipitated using cold acetone, and resuspended in Laemmli sample buffer in the same volume used for resuspending pellet fractions. Pellet and supernatant fractions were loaded onto a 10% polyacrylamide gel and resolved by SDS–PAGE. Proteins were stained using Coomassie Blue.

Electron microscopy

Actin polymerization was induced by adding salts to a final concentration of 100 mM KCl and 2 mM $MgCl_2$ into a G-actin preparation (Cytoskeleton) at 1 mg/ml and incubated at 22°C for 1 h. Vinculin (0.6 μM final concentration) and IpaA (0.1 μM final concentration) were added to F-actin (3.5 μM final concentration) and incubated for 2 h at room temperature in F′ buffer (15 mM Tris, 15 mM PIPES pH 7.0, 0.2 mM $CaCl_2$, 0.5 mM dithiothreitol, 0.2 mM ATP, 100 mM KCl and 2 mM $MgCl_2$). A few microliters of each sample were spotted onto a parafilm sheet. Formvas-coated copper grids were put down onto drops for 1 min, washed with uranyl acetate (1% in water) and allowed to dry on a filter paper. Grids were then rotary shadowed with 2–3 nm of platinium in a Balzers MED10 evaporater at 2×10^{-4} Pascal. Grids were observed with a Philips electron microscope at 60 kV.

Cell culture and microinjection

HeLa cells were grown in Dulbecco's modified Eagle's medium (DMEM; Gibco-BRL) with 10% fetal bovine serum (Gibco-BRL) at 37°C in an incubator supplemented with 5% CO_2, and seeded on glass coverslips (12 mm diameter, Marienfeld) 24 h prior microinjection. Purified IpaA was dialyzed against 25 mM Tris pH 7.3, 100 mM KCl, 5 mM $MgCl_2$, 1 mM EGTA, and microinjected at a concentration of 20 ng/μl into the cytoplasm of HeLa cells. IpaA was microinjected with FITC-labeled dextran (10 kDa, Molecular Probes) as a microinjection tracer, using an inverted microscope (IMT-2, Olympus) and a IM-200 microinjector (Narishige, USA, Inc.). For each sample, an average of 100 cells were microinjected over a 10 min period. Cells were then returned to the 37°C incubator for 5 or 15 min before fixation with paraformaldehehyde and fluorescence analysis. At least 100 microinjected cells were analyzed per sample and per incubation time, in at least two independent experiments.

Immunofluorescence microscopy

Cells were fixed in PBS containing 4% of paraformaldehyde (Sigma) for 20 min at 22°C and permeabilized using PBS containing 0.1% Triton X-100 (Sigma) for 4 min. Focal adhesions were stained using the anti-vinculin hvin1 monoclonal antibody (Sigma) and rhodamine-coupled anti-mouse IgG antibody (Jackson Immunoresearch) at a dilution of 1:200. F-actin was stained using rhodamine-coupled phalloidin (Sigma) at a dilution of 1:1000. Fluorescence microscopy analysis was performed using a direct microscope (BX50, Olympus).

Acknowledgements

We thank Kirsten Niebuhr for the gift of an anti-IpaA monoclonal antibody and Claude Parsot for providing the *ipaA* and *ipaB* mutant *Shigella* strains. We are grateful to all the members of the Unité de Pathogénie Microbienne Moléculaire for support and helpful discussions. We thank Jean-Christophe Olivo for assistance in videomicroscopy analysis. This work was supported by the 'Direction des Recherches et Techniques' (grant number 94092) and a grant to R.B.-S. from the 'Ministère de l'Education Nationale, de la Recherche et de la Technologie'.

References

Adam,T., Arpin,M., Prévost,M.-C., Gounon,P. and Sansonetti,P.J. (1995) Cytoskeletal rearrangements and the functional role of T-plastin during entry of *Shigella flexneri* into HeLa cells. *J. Cell Biol.*, **129**, 367–381.

Allaoui,A., Sansonetti,P.J. and Parsot,C. (1992) MxiD, an outer membrane protein necessary for the secretion of the *S.flexneri* Ipa invasins. *Mol. Microbiol.*, **7**, 59–68.

Clerc,P. and Sansonetti,P.J. (1987) Entry of *Shigella flexneri* into HeLa cells: evidence for directed phagocytosis involving actin polymerization and myosin accumulation. *Infect. Immun.*, **55**, 2681–2688.

Evans,R.R., Robson,R.M. and Stromer,M.H. (1984) Properties of smooth muscle vinculin. *J. Biol. Chem.*, **259**, 3916–3924.

Ezzell,R.M., Goldmann,W.H., Wang,N., Parasharama,N. and Ingber,D.E. (1997) Vinculin promotes cell spreading by mechanically coupling integrins to the cytoskeleton. *Exp. Cell Res.*, **231**, 14–26.

Gilmore,A.P. and Burridge,K. (1996) Regulation of vinculin binding to talin and actin by phosphatidylinositol-4-5-bisphosphate. *Nature*, **381**, 531–535.

Gilmore,A.P., Wood,C., Ohanion,V., Jackson,P., Patel,B., Rees,D.J.G. and Hynes,R.O. (1993) The cytoskeletal protein talin contains at least two distinct vinculin binding domains. *J. Cell Biol.*, **122**, 337–347.

Hayden,S.M., Miller,P.S., Brauweiler,A. and Bamburg,J.R. (1993) Analysis of the interactions of actin depolymerizing factor with G- and F-actin. *Biochemistry*, **32**, 9994–10004.

Hueck,C.J. (1998) Type III secretion systems in bacterial pathogens of animals and plants. *Microbiol. Mol. Biol. Rev.*, **62**, 379–433.

Hüttelmaier,S., Bubeck,P., Rüdiger,M. and Jockusch,B.M. (1997) Characterization of two F-actin-binding and oligomerization sites in cell-contact protein vinculin. *Eur. J. Biochem.*, **247**, 1136–1142.

Hüttelmaier,S., Mayboroda,O., Harbeck,B., Jarchau,T., Jockusch,B.M. and Rüdiger,M. (1998) The interaction of the cell-contact proteins VASP and vinculin is regulated by phosphatidylinositol-4,5-bisphosphate. *Curr. Biol.*, **8**, 479–488.

Jockusch,B.M. and Rüdiger,M. (1996) Crosstalk between cell adhesion molecules: vinculin as a paradigm for regulation by conformation. *Trends Cell Biol.*, **6**, 311–315.

Johnson,R.P. and Craig,S.W. (1994) An intramolecular association between the head and tail domains of vinculin modulates talin binding. *J. Biol. Chem.*, **269**, 12611–12619.

Johnson,R.P. and Craig,S.W. (1995) F-actin binding site masked by the intramolecular association of vinculin head and tail domains. *Nature*, **373**, 261–264.

Korneeva,N. and Jockusch,B.M. (1996) Light microscopic analysis of ligand-induced actin filament suprastructures. *Eur. J. Cell Biol.*, **71**, 351–355.

Kroemker,M., Rüdiger,A.-H., Jockusch,B.M. and Rüdiger,M. (1994) Intramolecular interactions in vinculin control α-actinin binding to the vinculin head. *FEBS Lett.*, **355**, 259–262.

Laemmli,U. (1970) Cleavage of structural proteins during the assembly of the head of bacteriophage T4. *Nature*, **227**, 680–685.

Lamb,J.A., Allen,P.G., Tuan,B.Y. and Janmey,P.A. (1993) Modulation of gelsolin function. Activation at low pH overrides Ca^{2+} requirement. *J. Biol. Chem.*, **268**, 8999–9004.

McGregor,A., Blanchard,A.D., Rowe,A.J. and Critchley,D.R. (1994) Identification of the vinculin-binding site in the cytoskeletal protein α-actinin. *Biochem. J.*, **301**, 225–233.

Ménard,R., Sansonetti,P.J. and Parsot,C. (1993) Non polar mutagenesis of the *ipa* gene defines IpaB, IpaC and IpaD as effectors of *Shigella flexneri* entry into epithelial cells. *J. Bacteriol.*, **175**, 5899–5906.

Ménard,R., Sansonetti,P.J. and Parsot,C. (1994) The secretion of the *Shigella flexneri* Ipa invasins is activated by epithelial cells and controlled by IpaB and IpaD. *EMBO J.*, **13**, 5293–5302.

Menkel,A.R., Kroemker,M., Bubeck,P., Ronsiek,M., Nikolai,G. and Jockusch,B.M. (1994) Characterization of an F-actin-binding domain in the cytoskeletal protein vinculin. *J. Cell Biol.*, **126**, 1231–1240.

Molony,L. and Burridge,K. (1985) Molecular shape and self-association of vinculin and metavinculin. *J. Cell. Biochem.*, **29**, 31–36.

Molony,L., McCaslin,D., Abernethy,J., Paschal,B. and Burridge,K. (1987) Properties of talin from chicken gizzard smooth muscle. *J. Biol. Chem.*, **262**, 7790–7795.

Otto,J.J. (1983) Detection of vinculin-binding proteins with an ^{125}I-vinculin gel overlay technique. *J. Cell Biol.*, **97**, 1283–1287.

Rodriguez Fernandez,J.L., Geiger,B., Salomon,D., Sabanay,I., Zöller,M. and Ben-Ze'ev,A. (1992) Suppression of tumorigenicity in transformed cells after transfection with vinculin cDNA. *J. Cell Biol.*, **119**, 427–438.

Rüdiger,M., Korneeva,N., Schwienbacher,C., Weiss,E. and Jockusch,B.M. (1998) Differential actin organization by vinculin isoforms: implications for cell type-specific microfilament anchorage. *FEBS Lett.*, **431**, 49–54.

Sansonetti,P.J., Kopecko,D. and Formal,S. (1982) Involvement of a plasmid in the invasive ability of *Shigella flexneri*. *Infect. Immun.*, **35**, 852–860.

Skoudy,A., Tran Van Nhieu,G., Mantis,N., Arpin,M., Gounon,P. and Sansonetti,P.J. (1999) A functional role for ezrin during *Shigella flexneri* entry into epithelial cells. *J. Cell Sci.*, **112**, 2059–2068.

Steimle,P.A., Hoffert,J.D., Adey,N.B. and Craig,S.W. (1999) Polyphosphoinositides inhibit the interaction of vinculin with actin filaments. *J. Biol. Chem.*, **274**, 18414–18420.

Tempel,M., Goldmann,W., Isenberg,G. and Sackmann,E. (1995) Interaction of the 47-kDa talin fragment and the 32-kDa vinculin fragment with acidic phospholipids: a computer analysis. *Biophys. J.*, **69**, 228–241.

Tran Van Nhieu,G., Ben-Ze'ev,A. and Sansonetti,P.J. (1997) Modulation of bacterial entry into epithelial cells by association between vinculin and the *Shigella* IpaA invasin. *EMBO J.*, **16**, 2717–2729.

Tran Van Nhieu,G., Caron,E., Hall,A. and Sansonetti,P.J. (1999) IpaC induces actin polymerization and filopodia formation during *Shigella* entry into epithelial cells. *EMBO J.*, **18**, 3263–3270.

Watarai,M., Funato,S. and Sasakawa,C. (1996) Interaction of Ipa proteins of *Shigella flexneri* with α5β1 integrin promotes entry of the bacteria into mammalian cells. *J. Exp. Med.*, **183**, 991–999.

Received June 29, 1999; revised and accepted September 10, 1999